Biomaterials Science

PAPER

View Article Online
View Journal

Cite this: DOI: 10.1039/c9bm01098j

Enhanced performance of chitosan/keratin membranes with potential application in peripheral nerve repair

Cristiana R. Carvalho,[a,b,c] João B. Costa,[a,b,c] Lígia Costa,[a,b] Joana Silva-Correia,[a,b] Zi Kuang Moay,[d] Kee Woei Ng,[d,e,f] Rui L. Reis[a,b,c] and Joaquim M. Oliveira[*a,b,c]

Although surgical management of peripheral nerve injuries (PNIs) has improved over time, autografts are still the current "gold standard" treatment for PNIs, which presents numerous limitations. In an attempt to improve natural biomaterial-based nerve guidance conduits (NGCs), chitosan (CHT), a derivative of the naturally occurring biopolymer chitin, has been explored for peripheral nerve regeneration (PNR). In addition to CHT, keratin has gained enormous attention as a biomaterial and tissue engineering scaffolding. In this study, biomimetic CHT/keratin membranes were produced using a solvent casting technique. These membranes were broadly characterized in terms of their surface topography and physicochemical properties, with techniques such as Fourier Transform Infrared Spectroscopy (FTIR), Differential Scanning Calorimetry (DSC), contact angle, weight loss and water uptake measurements, Scanning Electron Microscopy (SEM) and Atomic Force Microscopy (AFM). Biological *in vitro* assays were also performed, where a preliminary cytotoxicity screening with the L929 fibroblast cell line revealed that the membranes and respective materials are suitable for cell culture. In addition, Schwann cells, fibroblasts and endothelial cells were directly seeded in the membranes. Quantitative and qualitative assays revealed that the addition of keratin enhanced cell viablity and adhesion. Based on the encouraging *in vitro* results, the *in vivo* angiogenic/antiangiogenic potential of CHT and CHT/keratin membranes was assessed, using an optimized chick embryo chorioallantoic membrane assay, where higher angiogenic responses were seen in keratin-enriched materials. Overall, the obtained results indicate the higher potential of CHT/keratin membranes for guided tissue regeneration applications in the field of PNR.

Received 15th July 2019,
Accepted 9th October 2019

DOI: 10.1039/c9bm01098j

rsc.li/biomaterials-science

1 Introduction

Peripheral nerve injuries (PNIs) affect a vast number of the world population.[1] It has been estimated that approximately 2%–3% of all patients admitted to Level I trauma centers suffer from PNIs.[2] However, these injuries can result from traumatic or non-traumatic causes, where the correct diagnosis might not be performed. Therefore, it is difficult to estimate the real number of affected people. Still being one of the great challenges in the regenerative medicine field, PNIs cause significant sensorimotor impairment, disabling neuropathic pain and allodynia, which can last for a lifetime.[3] Furthermore, numerous studies suggest that functional and structural changes are caused in a patient's brain by PNIs and lead to devastating life-long consequences.[4]

After nerve injury, peripheral nerve regeneration is frequently and mistakenly believed to occur entirely. This is especially true when compared with nerve regeneration in the central nervous system (CNS), which is extremely limited. However, even with appropriate surgical treatment, severe incapacity often prevails after PNIs. In order to improve the limited functional outcomes, strategies focused on increasing the speed of axonal growth, maintaining Schwann cells in a healthy, repair-capable state and keeping target tissues receptive to reinnervation are required.[5]

[a]*3B's Research Group, I3Bs – Research Institute on Biomaterials, Biodegradables and Biomimetics, Headquarters of the European Institute of Excellence on Tissue Engineering and Regenerative Medicine, University of Minho, Avepark – Parque de Ciência e Tecnologia, Zona Industrial da Gandra, 4805-017 Barco, Guimarães, Portugal. E-mail: miguel.oliveira@i3bs.uminho.pt*
[b]*ICVS/3B's - PT Government Associated Laboratory, Portugal*
[c]*The Discoveries Centre for Regenerative and Precision Medicine, Headquarters at University of Minho, Avepark, 4805-017 Barco, Guimarães, Portugal*
[d]*School of Materials Science & Engineering, Nanyang Technological University, 50 Nanyang Avenue, 639798, Singapore*
[e]*Skin Research Institute of Singapore, 8A Biomedical Grove, 138648, Singapore*
[f]*Environmental Chemistry & Materials Centre, Nanyang Environment and Water Research Institute, 1 Cleantech Loop, 637141, Singapore*

Nowadays, nerve autografting, which consists in the implantation of a patient's own healthy nerves into the injured site, remains the gold standard treatment for peripheral nerve gaps longer than 5 mm.[6] To date, autografts have offered the best results in nerve regeneration under tension.[7] However, nerve autografts present several limitations such as donor tissue availability, loss of donor nerve function or formation of neuromas.[8] Consequently, there is an important need for the development of new and improved solutions for the treatment of PNIs.[9] In this context, artificial nerve guidance conduits (NGCs) and protectant nerve wraps (PNWs) can create a favourable microenvironment by mimicking the structure and composition of the peripheral nerve.[10] Membranes have also been used in guided tissue regeneration (GTR) to regulate tissue growth.[11] This method is based on the principle that a physical barrier is needed to stop the invasion of fast proliferating cells, such as collagen-depositing fibroblasts, while protecting the injury site.[12] This barrier will also provide an opportunity for more specific cells, such as Schwann cells and endothelial cells to migrate and participate in the regenerative process.

Until now, a variety of biomaterials have been studied for the repair of PNIs, including several natural and synthetic polymers.[13] Over the last few decades, greater importance has been given to naturally derived materials used in NGC, PNW and membrane development, which must be biologically active and show adequate biocompatibility and biodegradability.[7] These materials should also form systems as similar as possible to the extracellular matrix (ECM) and provide an increased rate of growth for the regenerating tissue.[6]

Chitosan (CHT), as a natural polysaccharide, has attracted increasing attention due to its biocompatibility, biodegradability, non-toxicity, ready availability and unique physicochemical properties.[14] Recent reports revealed the suitability of CHT materials as a substrate for peripheral nerve regeneration (PNR).[15] Briefly, *in vitro* biological evaluation revealed that CHT membranes sustained the survival, growth and alignment of different neuronal cells, such as neurons and Schwann cells, being suggestive of the potential use of CHT in neural Tissue Engineering (TE).[16] It has also been demonstrated *in vivo* that CHT NGCs could induce a notable motor and sensory functional recovery in rat sciatic nerve defects.[17] Furthermore, CHT constructs applied to long distance peripheral nerve defects performed comparably to autologous nerve grafting in rats.[18,19]

Recently, keratin extracted from human hair has emerged as a captivating biomaterial, which, as a human-derived protein, exhibits excellent biocompatibility, does not elicit an immune reaction upon transplantation, presents appropriate cellular-material interactions and biodegradability.[20] The progress in extraction, purification and characterization methods has boosted keratin as a potential scaffold material for biomedical applications.[21,22] Furthermore, it has been reported that a keratin molecule consists of approximately 400–600 amino acids and contains various cell-binding sites such as LDV (Leu-Asp-Val) and RGD (Arg-Gly-Asp), strongly supporting cell adhesion.[23,24] These molecular findings allowed keratin to be successfully used as a coating material for cell culture, resulting in an improvement of cell adhesion and proliferation.[20] Furthermore, the interest in keratin also arises from the fact that the hair follicle from which keratin is extracted is a remarkably proliferative organelle that shows a fast and continious regenerative process. However, keratin alone gives rise to very fragile materials or scaffolds, with poor strength and flexibility. Hence, polymer blending is an attractive method which is commonly used for providing polymeric materials with combined properties suitable for a specific application. Also, the addition of keratin to other biomaterials has been shown to modulate the viscoelastic and microstructural properties.

In the field of PNR, several studies with human hair keratin have been conducted in different animal models, from mice[25] and rats[26] to rabbits[27] and non-human primates.[28] Due to the visible success of a keratin hydrogel in promoting nerve repair, a phase I prospective, randomized trial is currently ongoing, entitled "Multicenter Clinical Trial of Keratin Biomaterial for Peripheral Nerve Regeneration" (ADA613738).

In this experimental work, we hypothesized the reinforcement of the biological and topographical potential of CHT membranes by blending them with keratin, envisioning its use in PNR. The resulting membranes were physicochemically characterized in terms of their surface topography by SEM and AFM, as well as their chemical features, by FTIR and DSC, and degradation, swelling and contact angle measurements, in order to confirm if the blending was successfully achieved. Afterwards, *in vitro* culture studies for cell behavior analysis were carried out using three human cell types that play key roles in the PNR process: skin fibroblasts, Schwann cells and endothelial cells. Since vascularization is a vital and limiting process in PNR, the chick embryo chorioallantoic membrane (CAM) assay was carried out to investigate the angiogenic potential of the developed materials.

According to our knowledge of the literature, this is the first time that keratin has been blended with CHT in order to improve the biological and physicochemical properties of biomaterials, with the specific application of PNR in mind. The idea was to synergistically take advantage of both polymers and study if their physicochemical and biological characterization would match the requirements necessary for use in peripheral nerve repair and regeneration. Along with the characterization, it was realized that the performance of both Schwann cells and endothelial cells was significantly improved in the presence of keratin. Furthermore, it was also demonstrated for the first time, resourcing to a CAM assay, that the presence of keratin blended with CHT significantly enhanced blood vessel formation, which is critical for the success of nerve repair, especially in critically large gaps, where hypoxia is a detrimental factor hindering nerve repair.

2 Materials and methods

2.1 Materials

Alamar Blue was purchased from Invitrogen™; phosphate buffer saline, acetic acid, sodium hydroxide, sodium sulphide,

phalloidin, M199 medium, 4′,6-diamidino-2-phenylindole (DAPI), formalin, haematoxylin and eosin and heparin were purchased from Sigma-Aldrich; and an MTS kit and filter paper were purchased from Promega. Glutamax and penicillin/streptomycin (100 U/100 g mL^{-1}) were purchased from Life Technologies; an endothelial cell growth supplement (ECGS – 25 μg mL^{-1}) was acquired from Becton Dickinson; fertilized chicken eggs were acquired from Pintobar, Portugal; an UltraVision Large Volume Detection System Anti-Polyvalent was acquired from LabVision Corporation; citrate buffer was purchased from Merck; hydrogen peroxide was brought from Panreac; and SNA-lectin and 3,3′-diaminobenzidine (DAB) solution were purchased from Vector Laboratories.

2.2 Manufacture of CHT powder

Medical grade CHT powder supplied by Altakitin S.A. (Ki2Med®, Lisbon, Portugal) with a molecular weight (MW) of 260 kDa and a degree of acetylation (DA) of 5% was obtained from *Pandalus Borealis* shrimp shells using standard conditions for chitin extraction and deacetylation, following ISO 13485 requirements and specifications. The purification method consisted in homogeneous washing (liquid/liquid extraction) of CHT with EDTA and SDS for heavy metal and protein removal. After the extraction, the product was washed with deionized water and neutralized prior to lyophilization. The product was provided after analyses using several methods and techniques to attest compliance with internal standards for the degree of acetylation, molecular weight, heavy metal content, protein content, endotoxins, bioburden, pH, ash content and apparent viscosity.

2.3 Extraction of keratin from human hair

Random human hair samples were obtained from hair salons in Singapore and processed as previously described,[29] with minor modifications. Briefly, after washing the hair samples with soap and ethanol, delipidization was performed with a mixture of chloroform and methanol at a ratio of 2 : 1, for 24 hours. The delipidized hair was thoroughly air-dried to remove the organic solvents and snipped into fragments as small as 1–2 mm for keratin extraction. The hair fragments (45 g) were immersed in 1 L of 0.125 M sodium sulphide solution in deionized water and incubated at 40 °C for 4 hours. The resulting solution was filtered and extensively dialyzed against deionized water using membranes of 10 kDa molecular mass cut-off to remove residual sodium sulphide. The dialyzed solution was subsequently freeze-dried to obtain keratin powder and stored at −20 °C until use. To ensure sterility, the whole process was conducted in a class II biosafety cabinet and all solutions were sterile-filtered. Typical yields were calculated to be between 20 and 40% by weight percentage. Based on this extraction protocol, the protein fraction obtained was previously shown to contain both monomers of Type 1 and 2 hair keratins in the molecular weight range of 45–60 kDa,[30] which retain the typical peptide bond profiles expected for intact proteins.[31]

2.4 Preparation of CHT and CHT/keratin membranes

Ki2Med® CHT powder with 5% DA was dissolved in 0.25 M acetic acid aqueous solution to attain a final concentration of 2%wt. For the samples containing keratin, the freeze-dried powder was added to the previous solution to achieve a 2% CHT/1%wt keratin solution. The solutions were stirred overnight and filtered to remove impurities. After casting onto Petri dishes, the samples were dried for at least 5 days at room temperature (RT). The dried membranes were neutralized in 0.25 N sodium hydroxide and washed every 30 minutes until reaching neutral pH, and further dried at room temperature in the respective molds. All membranes were sterilized with ethylene oxide (EO) gas, considered by some authors the most suitable method of sterilization for CHT membranes.[32]

2.5 Physicochemical characterization of CHT and CHT/keratin membranes

2.5.1 Membrane thickness measurement. The membrane thickness was measured with a digital micrometer (Mitutoyo, Japan). Five membranes were used. The results are expressed as mean ± standard deviation.

2.5.2 Surface evaluation by stereomicroscopy, scanning electron microscopy (SEM) and atomic force microscopy (AFM). Three CHT and CHT/keratin membranes were cut into 1 cm^2 samples. The developed membranes were examined under a stereomicroscope + lamp (Schott KL 200, model Stemi 1000, Zeiss) for a macroscopic inspection of their topography and general aspects.

For SEM, the membranes were sputter coated with gold for the analyses of their surface morphology (model S360, Leica, Cambridge, England).[33] For surface roughness analysis, the membranes were analysed on five spots using TappingMode™ with a MultiMode connected to a NanoScope III (Veeco, USA) and non-contacting silicon nanoprobes (TESP model, Bruker). The images (10 μm × 10 μm wide) were fitted to a plane using the first-degree flatten procedure included in the NanoScope software version 4.43r8. The surface roughness was calculated as Rq (root mean square from average flat surface) and Ra (average absolute distance from average flat surface).[34]

2.5.3 Fourier transform infrared spectroscopy (FTIR). FTIR spectra of keratin powders, as well as CHT and CHT/keratin membranes, were obtained using a Shimadzu IRPrestige 21 spectrometer (IRPrestige-21, Shimadzu, Japan). All spectra were acquired at room temperature by averaging 32 scans at a resolution of 4 cm^{-1} and a wavelength range of 400–4000 cm^{-1}.[35]

2.5.4 X-ray diffraction (XRD). X-ray diffraction patterns of keratin powder, CHT and CHT/keratin membranes were used to determine their crystalline structures. Measurements were performed in a Bruker D8 Advance Davinci diffractometer equipped with a Cu Kα radiation source (λ = 1.547 Å), with radiation produced at 40 kV and 40 mA. The data were collected at room temperature, with an increment of 0.02°, a 2θ

range of 5–40° and the increment's acquisition time of 1 second.[36]

2.5.5 Contact angle measurements: wettability and surface energy determination. The surface properties of CHT and CHT/keratin membranes were studied through static contact angle (θ) measurements using the sessile drop method[37] with ultra-pure distilled water (as a polar liquid) and diiodomethane (as a non-polar liquid) (OCA equipment, Germany and SCA-20 software). Five measurements were carried out for each sample. Considering the contact angle measurements, the surface energy was calculated using the Owens, Wendt, Rabel and Kaelble (OWRK) equation.[38] During every determination, a motor-driven syringe was used to deposit a drop of the liquid over the membrane surface. The images corresponding to these drops were properly recorded and analyzed. The different determinations were performed at RT and in triplicate.

2.5.6 Dynamic mechanical analysis (DMA). The viscoelastic measurements of the CHT and CHT/keratin membranes were performed using a TRITEC8000B DMA (Triton Technology, UK), in tensile mode. All samples were immersed in phosphate buffer saline (PBS) solution before measurement and left overnight at 37 °C. DMA spectra were acquired with a frequency scan ranging between 0.1 and 15 Hz for all time points. The experiments were performed under a constant strain amplitude, corresponding to approximately 2% of the original height of the sample. Five samples were tested under physiological conditions.[39]

2.5.7 Differential scanning calorimetry (DSC). DSC analysis was performed on a DSC Q100 apparatus (TA Instruments Inc, USA). The samples were packed in a TA aluminum pan (3–6 mg sample weight), which was covered with a suitable aluminum cover. Both temperature and heat flux were previously calibrated with indium. Both samples were subjected to ramp heating ranging from 0 °C to 350 °C at a rate of 5 °C per minute. The measurements were performed under a dry nitrogen atmosphere, at a flow rate of 50 mL per minute.[40]

2.5.8 *In vitro* weight loss and water uptake profiles. *In vitro* weight loss by hydrolysis and water uptake profiles of CHT and CHT/keratin membranes were evaluated through immersion in PBS, under dynamic conditions (60 rpm) in a water bath at 37 °C, for a period up to 30 days.[41] After determined timepoints (*i.e.* 0, 7, 14, 21 and 30 days) the excess of surface water was removed with filter paper. Afterwards, the membranes were left to dry completely at 60 °C and the weight of the sample was measured. The weight loss percentage of the membranes was calculated using eqn (1):

$$\text{Weight loss}(\%) = \frac{(m_i - m_f)}{(m_i)} \times 100\% \quad (1)$$

where, m_f is the sample weight at the end of the assay, and m_i is the initial weight of the dry sample. For water uptake determination, at each timepoint, the excess of surface water was removed with filter paper and the weight of the sample was measured. The water uptake percentage was calculated using eqn (2):

$$\text{Water uptake}(\%) = \frac{(m_w - m_i)}{(m_i)} \times 100\% \quad (2)$$

where, m_i corresponds to the initial weight of the dry sample and m_w to the wet weight of the sample after removal from solution, at each timepoint. The average value of three measurements was considered for each assay.

2.6 *In vitro* biological studies

2.6.1 Cell culture. L929 mouse lung fibroblasts (from the European Collection of Cell Cultures (ECCC)), human skin fibroblasts (BJ, CRL-2522, ATCC), immortalized human Schwann cells (iSCs, sNF96.2, ATCC) and human pulmonary microvascular endothelial cells (HPMEC-ST1.6R cell line) were cultured as monolayers at 37 °C under a humidified 5% CO_2 atmosphere. L929 fibroblasts were incubated with low glucose Dulbecco's Modified Eagle's Medium (DMEM), supplemented with 10% (v/v) FBS and 1% (v/v) penicillin/streptomycin. Human skin fibroblasts were incubated with Eagle's Minimum Essential Medium (EMEM), supplemented with 10% (v/v) FBS, 1% (v/v) penicillin/streptomycin and 1% sodium pyruvate. Immortalized Schwann cells were cultured under the same conditions but incubated with high glucose DMEM supplemented with 1% (v/v) sodium pyruvate. HPMEC-ST1.6R endothelial cells were cultured in M199 medium supplemented with 20% (v/v) FBS, 2 mM Glutamax, 2% (v/v) penicillin/streptomycin, 50 μg mL^{-1} of heparin and 25 μg mL^{-1} of the endothelial cell growth supplement (ECGS).[42] The cellular expansion medium was exchanged every 2–3 days until confluency was achieved.

2.6.2 Short-term cytotoxicity screening and adhesion study. L929 fibroblasts were used in these preliminary cytotoxicity and adhesion assays. To assess the short-term cytotoxicity of the developed membranes, a previously described protocol was used,[43] which makes use of MEM extraction followed by MTS assay. This assay is particularly effective at determining the possible toxic effects of conditioned media released from medical polymers during extraction, following ISO 10993-5. For this, CHT and CHT/keratin membranes were incubated with complete DMEM for 24 hours, at 37 °C and 60 RPM, where the ratio of the material weight to extraction fluid was constant and equal to 0.2 g mL^{-1}. At the same time, L929 fibroblasts were seeded in a 24-well plate at the density of 5×10^4 per well and cultured with complete DMEM for 24 hours at 37 °C under an atmosphere with 5% CO_2. After 24 hours of incubation, the CHT and CHT/keratin extracts were filtered through a 0.45 mm pore size filter. The culture medium was removed from the wells and an identical volume of conditioned medium (1 mL) was added. The metabolic cell activity (an indirect measure of cytotoxicity) was measured by the conversion of MTS to formazan, which can be photometrically detected. The cell response in terms of metabolic viability was evaluated after 24, 48, and 72 hours of incubation time. At

each timepoint, the extraction fluid was removed and 500 mL of a mixture of serum-free culture medium without phenol red and MTS reagent (5 : 1 ratio) was added to each well. A monolayer of cells seeded in Tissue Culture Polystyrene (TCP) in culture medium was used as a positive control, since it represents the ideal situation for cell proliferation. Latex was used as a negative control (for cell death). All experiments were performed in triplicate and the sample left to incubate for 3 hours at 37 °C under a humidified 5% CO_2 atmosphere. Thereafter, the absorbance of each sample was measured in triplicate at 490 nm using a microplate reader (Synergy HT, Bio-TEK). The MTS assay was repeated 3 times.

A preliminary qualitative and quantitative study of cellular adhesion was performed 3, 6, 8 and 24 hours after seeding of L929 fibroblasts in CHT and CHT/keratin membranes. At each timepoint, cells were fixed with a 10% (v/v) formalin solution and dyed with DAPI (4′-6-diamidine-2-phenylindole) to visualize the nuclei (blue colour) and phalloidin, which binds to the cell cytoplasm F-actin (red colour). For the quantitative analyses, the area occupied by the cells (μm^2) under each condition was calculated using ImageJ software (Fiji), after applying a suitable threshold, in order to evaluate the differential adhesion in the CHT and CHT/keratin membranes.

2.6.3 Cellular viability quantification in 2D cultures of relevant cell types. For the Alamar Blue (AB) assay, BJ fibroblasts, immortalized Schwann cells and endothelial cells were seeded separately in 1 cm^2 CHT and CHT/keratin membranes, placed in the bottom of 24-well cell culture plates, at a density of 5×10^4 cells/membrane. The samples were analysed after 1, 3 and 7 days of culturing at 37 °C under a humidified 5% CO_2 atmosphere using the corresponding culture medium. At each timepoint, the respective cell culture medium containing 10% AB was added to the different culture wells and the systems were incubated for 3 hours. Afterwards, 100 μL of each solution were transferred in triplicate to white opaque 96-well plates. Fluorescence was read at a 590 nm emission wavelength (excitation wavelength: 530 nm), using the microplate reader (FL 600, Bio-Tek Instruments). Since AB is non-cytotoxic, the same cells' seeded membranes were used through the entire 7 days of culturing.[44] PBS was used for removing the AB reagent from the samples and was replaced by fresh medium after each AB determination. Normalization was performed by using the mean fluorescence value obtained for the TCPs, with and without cells.

2.6.4 Cellular cytoskeleton morphology study of relevant cell lines. The cell morphology was studied through fluorescence microscopy after fixing the samples used in the AB assay (after 1, 3 and 7 days in culture), with 10% (v/v) formalin solution. Staining with phalloidin and DAPI (4,6-diamidino-2-phenylindole dilactate) was performed following suppliers' protocol. The dye was removed by washing with PBS and the samples were analysed by means of using a transmitted and reflected light microscope (Axio Imager Z1 m, Zeiss, Jena, Germany).

2.7 *In vivo* angiogenesis evaluation

2.7.1 Chick embryo chorioallantoic membrane (CAM) assay. CAM assay was performed according to the procedure described by Silva-Correia *et al.*[45] in a laminar-flow hood. White fertilized chicken eggs (n = 90–120) were incubated at 37 °C for 3 days. Afterwards, a small hole was created in the endpoints of the egg to permit detachment of the CAM from the shell membrane. Additionally, a spherical hole was made into the eggshell, in order to evaluate embryo viability and access the CAM. The shell window was then sealed with tape to prevent dehydration and the eggs were returned to the incubator until implantation of the CHT and CHT/keratin membranes (cut in 4 mm-diameter circles). A total of three experimental groups were tested. CHT and CHT/keratin sterile membranes were implanted on the CAM at day 10 of embryonic development. At the same time, a positive control group was also implanted on the CAM, which was based on filter paper (FP). The shell windows were protected with tape and the eggs returned to the incubator until day 14 of embryonic development. At the end of the assay, the embryos and their membranes were fixed *in ovo* by using freshly prepared formalin solution at 4% (v/v) followed by incubation at −80 °C for 10 minutes. The implanted materials and the adjacent CAM portions were cut and transferred to 6-well plates containing 4% formalin solution. *Ex ovo* images were acquired using the AxioVision imaging software (release 4.8; Zeiss) connected to an AxioCAM ICc1 digital camera (Zeiss) attached to a stereomicroscope (Stemi 2000-C; Zeiss). The excised membranes were transferred to histological cassettes, embedded in paraffin and cut into sections of 4 mm thickness using a microtome (Spencer 820, American Optical Company, NY, USA). Three independent CAM assays were performed.

2.7.2 Analysis of blood vessel convergence. To evaluate the total number of macroscopic blood vessels converging toward the implanted materials (CHT, CHT/keratin membranes and FP), a semi-quantitative method was used, as previously described by Ribatti *et al.*[46] The number of convergent blood vessels were counted in the *ex ovo* images obtained at day 14 of embryonic development, after image processing using the WCIF ImageJ software program (US National Institutes of Health). The mean number of blood vessels results from the counts performed by three independent observers of a minimum of 19 discs per implant.

2.7.3 Hematoxylin & eosin (H&E) staining. The CAM sections were stained with H&E and observed under transmitted microscopy using an Axio Imager Z1 m light microscope (Zeiss, Jena, Germany). Images were acquired using the Zen microscope processing software (Zeiss, Jena, Germany) connected to a digital camera AxioCam MRc5 (Zeiss, Jena, Germany).

2.7.4 Immunohistochemical detection. A regular immunohistochemical protocol was used as described: after paraffin removal, the sections were rehydrated and subjected to heat-induced antigen retrieval using 10 mM citrate buffer (pH 6.0) for 20 minutes at 98 °C. To inactivate endogenous peroxidases,

the samples were incubated in 3% hydrogen peroxide solution for 10 minutes and then soaked in PBS. The sections were incubated in protein blocking solution for 10 minutes, followed by incubation with lectin (SNA, EBL) for 1 hour at room temperature. To conclude, the sections were consecutively washed with PBS and incubated with a streptavidin-peroxidase complex for 10 minutes. DAB solution was used as a chromogen. All sections were counterstained with hematoxylin (modified Mayer's). The histological sections were analyzed, and images acquired as described in 2.7.3.

2.8 Statistical analysis

All the numerical results were presented as mean ± standard deviation. At least 3 specimens were used under each condition. Statistical analysis of the data was conducted using the GraphPad Prism Software version 5.00 for Windows (GraphPad Software, Inc., La Jolla, USA). For AFM data analysis, a minimum of 3 samples were used and a two-tailed Mann Whitney test was performed ($p < 0.05$). Results from *in vitro* tests were analyzed for normality of data distribution by the Shapiro–Wilk normality test, followed by the Kruskal Wallis test in order to compare the results from the different groups. Three independent experiments were performed ($n = 3$). The quantitative study of the convergent blood vessels was analyzed first by the Shapiro–Wilk test to access the normal distribution of data, followed by one-way analysis of variance (ANOVA) and Tukey's multiple comparisons test. Three independent experiments were performed ($n = 3$). The significance level was set to $*p < 0.05$, $**p < 0.01$, $***p < 0.001$, $****p < 0.0001$ in all the experiments.

3 Results

3.1 Physicochemical characterization

3.1.1 Membrane thickness. In order to assess if the addition of keratin would lead to any changes in the thicknesses of membranes, five samples of each formulation were tested. The CHT and CHT/keratin membrane thickness was 505.8 ± 5.34 μm and 506.2 ± 5.98 μm, respectively. Therefore, no statistical significance related to the addition of keratin was found regarding the thicknesses of the membranes.

3.1.2 Microstructure evaluation. Stereomicroscopy photographs revealing the surface macrostructure of the CHT-based membranes can be seen in Fig. 1A. In Fig. 1Ai, the CHT membrane surface appears to be smooth, while the incorporation of freeze-dried keratin powder leads to an irregular and rough surface (Fig. 1Aii). When comparing both surfaces (Fig. 1Aiii), it is clear that there is an increase of roughness in the presence of keratin. This contrasts with the smooth surface of the CHT membrane.

SEM microphotographs of CHT (Fig. 1Bi and ii) and CHT/keratin (Fig. 1Biii and iv) membranes confirmed the stereomicroscopy observation, revealing that the incorporation of keratin induced the formation of a rough area with grooves, ridges and heterogeneous porous microstructures with a pore

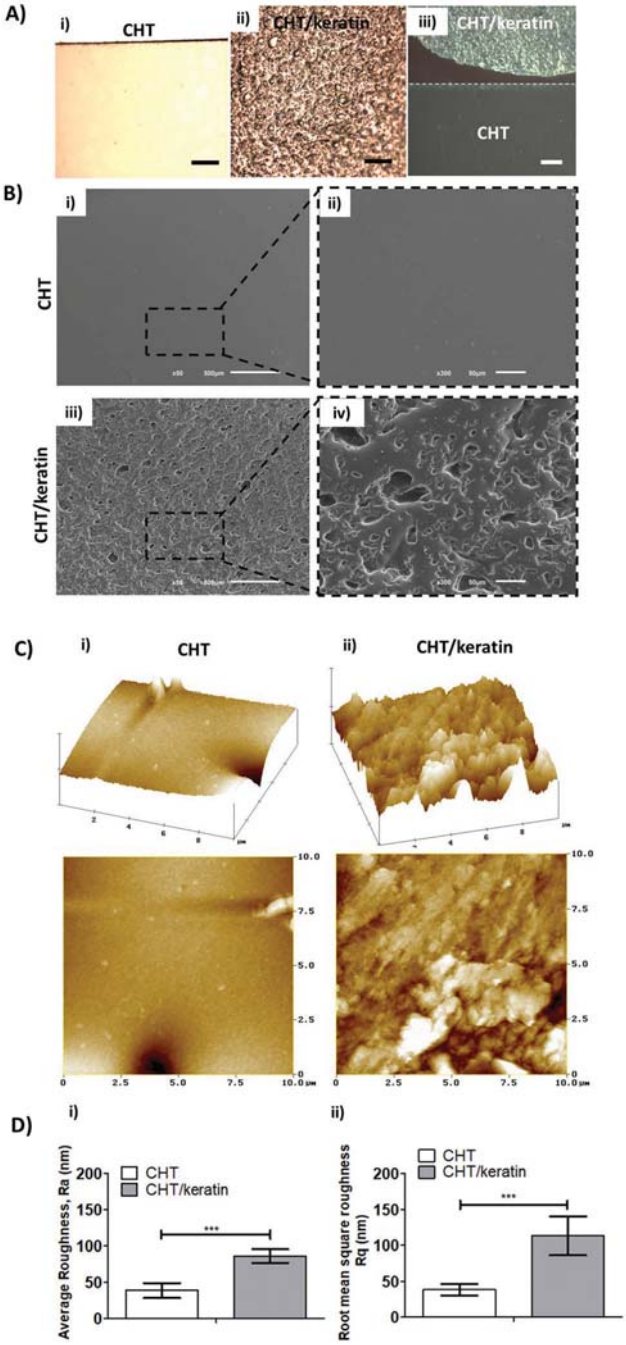

Fig. 1 Macro- and microphotographs of the developed CHT and CHT/keratin membranes revealing their surface topography. (A) Photographs of the membranes taken with a stereomicroscope: (i) the smooth surface of the CHT membrane, (ii) the rough surface of the CHT/keratin membrane, and (iii) comparison between CHT and CHT/keratin membranes; (B) SEM microphotographs of the developed membranes: (i–ii) CHT membrane and (iii–iv) CHT/keratin membrane; (C) AFM three-dimensional images of the developed membranes, 10 μm × 10 μm scan area, contact mode of (i) CHT and (ii) CHT/keratin; and (D) quantitative information regarding the average roughness (R_a) and root mean square roughness (R_q) of the (i) CHT and (ii) CHT/keratin membranes. Two-tailed Mann Whitney Test was used ($p < 0.05$) and statistically significant differences were represented by *** ($p < 0.001$). Scale bars: (A) 500 μm and (B) 500 μm (i and iii) and 50 μm (ii and iv).

size in the range of 3–100 μm. Conversely, the CHT membranes are flat and smooth. The detailed surface structure of the membranes can be seen in the magnification images on the right (Fig. 1Bii and iv). The surface topography of CHT and CHT/keratin membranes was qualitatively and quantitatively studied by AFM (Fig. 1C and D, respectively). AFM provides a 3D profile on a nanoscale, by measuring forces between a sharp probe and the surface of the samples, at a very short distance (0.2–10 nm probe-sample). To evaluate the roughness of the samples, parameters such as R_a and R_q were automatically calculated with the software Nanoscope III. R_q is the root mean square average of height deviation, taken from the mean image data plane. R_a is the arithmetic average of the absolute values of the surface height deviations measured from the mean plane. Visually and qualitatively, the difference between both membranes is striking. These results confirm the findings obtained from SEM. Quantitatively, for CHT/keratin membranes, the average roughness (R_a) was calculated to be 86.04 ± 8.31, whereas a significantly lower value was obtained for the CHT membrane (38.58 ± 9.4) (Fig. 1Di). Similarly, a higher value of root mean square roughness (R_q) was obtained for the CHT/keratin membrane (113.5 ± 24.4), as compared to the CHT membrane (38.3 ± 7.4) (Fig. 1Dii). Therefore, the results demonstrate that a significantly higher roughness of the CHT/keratin membranes (both R_a and R_q) is observed at the nanoscale level.

3.1.3 FTIR results. FTIR was used to confirm the presence of functional groups of both components, *i.e.* CHT and keratin, after the blending and to exclude any possible chemical modification induced by the blending and manufacturing processes. FTIR spectra are presented in Fig. 2A. On one hand, the keratin powder spectrum showed its fundamental characteristic peaks, *i.e.* the band in the range of 1600 cm^{-1}, which corresponds to amide I and is mainly related to C═O stretching, and the band in the range of 1500 cm^{-1}, which suggests the presence of amide II and results from the phase combination of C–N stretching and C═O bending vibrations. On the other hand, the chitosan spectrum of a pure CHT membrane has a band at 3441 cm^{-1}, which corresponds to the combined peaks of the NH_2 and OH group stretching vibrations. The bands at 1640 cm^{-1} and 1380 cm^{-1} correspond to the C═O and C–O stretching of the amide group. The characteristic features of the chitosan spectrum in this study are similar to those of previous reports.[47,48] As expected, in the spectra of the CHT/keratin membrane an increase of the intensity of the amide I and amide II bands (1600 and 1500 cm^{-1}, respectively) was observed, due to the presence of keratin in CHT membranes.

3.1.4 XRD results. The XRD profiles of CHT and CHT/keratin membranes and keratin powder are shown in Fig. 2B. The characteristic peaks of the CHT membrane appear at around 15° and 20°.[49] Fahmy *et al.*[50] reported that the reflection at 2θ = 15° is assigned to the crystal form I and attributed to the hydrated crystals with low crystallinity. That study also reported that this peak may shift from 9° to 15°. The peak at 2θ = 20° represents the crystallinity of the crystal form II in the CHT structure. In the keratin powder spectrum presented in Fig. 2B (superior right corner), two intense peaks can be visualized at 2θ = 10° and 2θ = 20°, which are assigned to both α-helix and β-sheet structures of keratin, respectively, pointing towards the crystalline properties of the protein.

After the blending, instead of an intense peak at 2θ = 10°, there is only a small peak which indicates that the final CHT/keratin membrane has a relatively lower α-helix and crystallinity than the freeze-dried keratin powder. Overall, the addition of keratin to the chitosan membrane leads to a decrease in crystallinity, due to a lower degree of molecular order.

3.1.5 Contact angle and surface energy measurements. The hydrophobic/hydrophilic nature of CHT and CHT/keratin membranes was assessed by means of performing contact angle measurements (Table 1). The results indicated that the CHT/keratin membrane has a higher polar component and surface energy, corresponding to a lower water contact angle, when compared to CHT membranes. The CHT/keratin membrane was found to be more hydrophilic, presenting a water contact angle value of 101.06 ± 5.35 and a surface energy of 29.04 ± 0.01 of. Meanwhile, the CHT membrane presented a water contact angle value of 115.2 ± 1.96 and a surface energy of 25.22 ± 0.01.

3.1.6 DMA analysis. Experiments were performed in a hydrated environment at 37 °C, in an array of biologically relevant frequencies, in order to assess the behavior of samples in physiological-like setting. Both storage (elastic) modulus, E', and the loss factor, $\tan\delta$, were obtained at different frequencies. The E' is a measure of the stiffness of the materials. The loss factor corresponds to the ratio of the amount of energy dissipated (viscous component) relative to the energy stored (elastic component); $\tan\delta = E'/E''$. CHT and CHT/keratin properties are shown in Fig. 2C. The values of the storage modulus (E') for CHT membranes presented a slight increase from 68.8 ± 5.8 MPa to 77.7 ± 9.8 MPa, as the frequency increased from 0.1 to 10 Hz. In the same range of frequencies, CHT/keratin membranes revealed lower storage modulus values. For this sample, the storage modulus remained relatively constant in the range of frequencies tested, presenting values from 40.1 ± 6.7 MPa to 41.7 ± 4.2 MPa. Regarding the loss factor results ($\tan\delta$), CHT/keratin presented higher values compared to simple CHT membranes. A decrease from 0.74 ± 0.07 to 0.66 ± 0.09 and from 0.48 ± 0.05 to 0.41 ± 0.07 was observed for CHT/keratin and CHT membranes, respectively, as the frequency increased. After statistical analyses, it was found that there is a statistically significant difference between the storage modulus and the loss factor of CHT and CHT/keratin at a frequency of 1 Hz. This value corresponds to the frequency related to the movement of walking (ambulatory frequency).

3.1.7 DSC analysis. A DSC thermogram of CHT and CHT/keratin membranes, as well as keratin powder, is shown in Fig. 2D. The intense endothermic peak verified at 50 °C in the keratin powder thermogram is related to the evaporation of water of the freeze-dried powder. It is worth noting that in the keratin powder, water evaporation occurs at lower temperature, as compared to CHT and CHT/keratin membranes (50 °C in

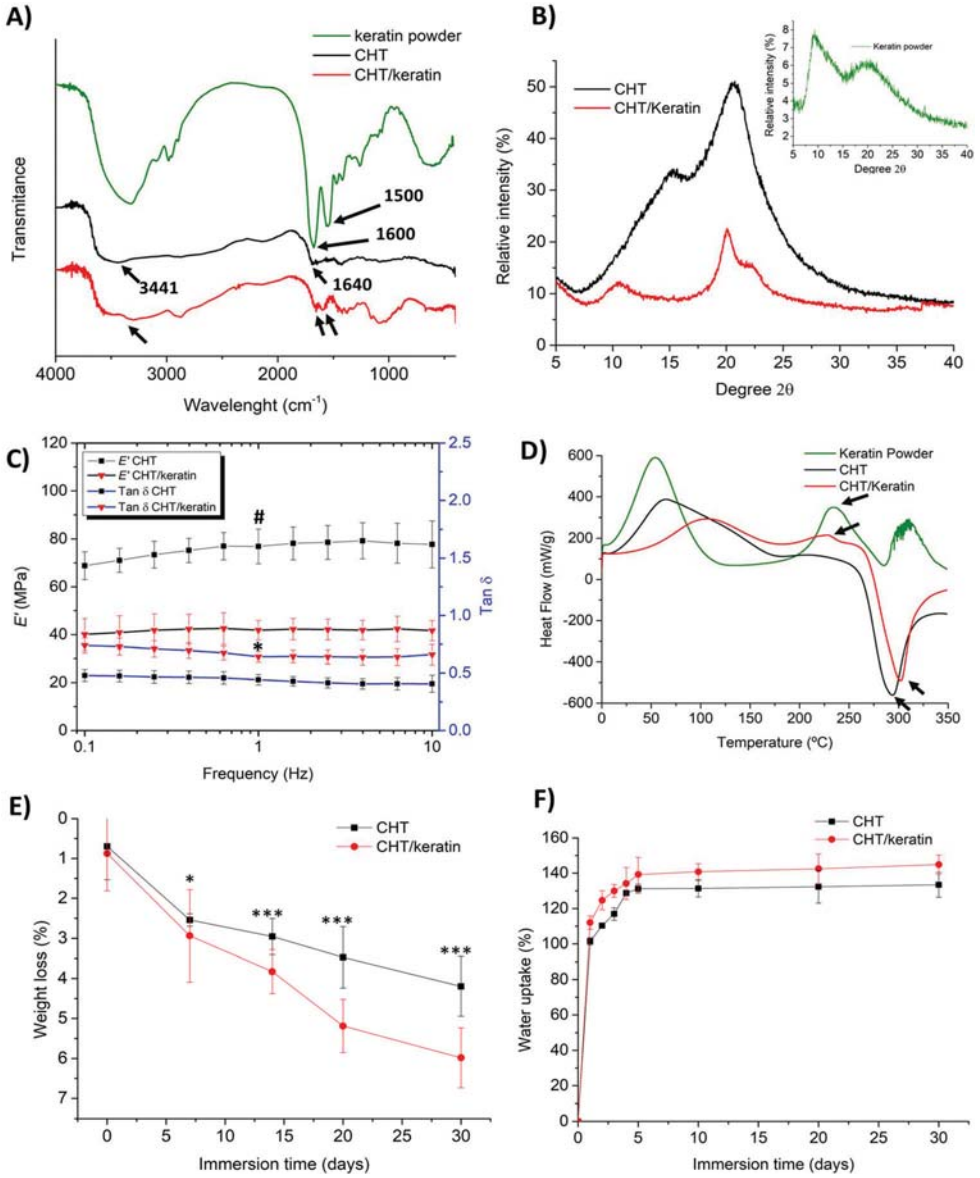

Fig. 2 Physicochemical characterization of CHT and CHT/keratin membranes. (A) FTIR spectra of the produced membranes and keratin powder. Arrows point to specific and characteristic peaks of each component, which are also visible in the final blending membrane; (B) XRD pattern of the produced membranes. In the upper right side (green line), at a different scale, is the XRD pattern of keratin powder; (C) dynamic mechanical analysis of the membranes. Storage modulus (E', black lines) and loss factor (tan δ, blue lines) of samples measured as a function of frequency; # represents statistically significant difference between the storage moduli of CHT and CHT/keratin at 1 Hz (* ($p < 0.05$). * represents statistically significant difference between the loss factors of CHT and CHT/keratin at 1 Hz (** ($P < 0.01$); and (D) differential scanning calorimetry thermograms of the developed membranes. Arrows point to specific and characteristic peaks of each component, which are also visible in the final blending membrane. (E) Percentage of weight loss of the developed membranes after incubation in PBS for different periods of time. The data represent the mean for each timepoint ± standard deviation; statistically significant differences were found between CHT and CHT/K at 7, 14, 20 and 30 days after immersion in PBS, where the statistical significance level was set to *$p < 0.05$, **$p < 0.01$ and ***$p < 0.001$. (F) Percentage of water uptake of the developed membranes after incubation in PBS for different periods of time. The data represent the mean for each timepoint ± standard deviation. No statistically significant differences were found between the samples at any timepoint studied.

the keratin powder and 70–100 °C in the CHT/keratin membranes). This can be related to the high tendency of water absorption from the freeze-dried powder, which promotes its evaporation at lower temperatures. In the keratin powder thermogram, an endothermic peak around 240 °C is also visible, which appears due to protein denaturation, more specifically, denaturation of the α-helix of keratin. This same peak is visible in the CHT/keratin blend, although with less intensity. In both CHT and CHT/keratin membranes, the presence of intense peaks at 300 °C was observed, which are associated with the decomposition of the amine units in the chitosan structure.

Table 1 Contact angles (θ), dispersive (γ_d) and polar (γ_p) components and surface energy (γ) of the CHT-based membranes calculated using the OWRK equation

Material	θ_{water} (°)	γ_d (mN m^{-1})	γ_p (mN m^{-1})	γ (mN m^{-1})
CHT membrane	115.2 ± 1.96	34.61 ± 0.01	0.61 ± 0.00	25.22 ± 0.01
CHT/keratin membrane	101.06 ± 5.35	18.60 ± 0.01	0.93 ± 0.00	29.04 ± 0.01

3.1.8 Weight loss and water uptake profiles. The weight loss of the developed membranes was evaluated in PBS (at pH 7.4). From Fig. 2E, it can be observed that CHT and CHT/keratin follow a similar pattern of degradation with time. The weight loss was minimum after 1 day, with values of 0.70 ± 0.53% and 0.9 ± 0.3% for CHT and CHT/keratin, respectively. The weight loss gradually increased from 2.54 ± 0.16% to 4.19 ± 0.75% in the CHT sample, from day 7 to day 30. In the same time period, the CHT/keratin sample degraded from 2.9 ± 1.2% to 6.0 ± 0.7%. Statistically significant differences were found between CHT and CHT/K at 7, 14, 20 and 30 days after immersion in PBS.

The water uptake of the membranes is presented in Fig. 2F. The swelling of both samples was found to reach its maximum and stabilize after 5 days of immersion, with values of 131.2 ± 2.5% and 139.2 ± 9.7% for CHT and CHT/keratin samples, respectively. No statistically significant differences were found between the samples at any timepoint studied regarding the water uptake.

3.2 *In vitro* studies

3.2.1 Short-term cytotoxicity screening and adhesion study. Conditioned media (extracts) obtained from CHT and CHT/keratin membranes did not demonstrate any cytotoxic effect on L929 cells after 24, 48 and 72 hours of incubation, as shown in Fig. 3A. There are no statistically significant differences in the MTS results regarding both membranes and the positive control, irrespective of the timepoint analysed. The qualitative adhesion assay suggests a relatively higher adhesion of L929 cells to keratin-containing membranes, during several timepoints (3, 6, 8 and 24 hours).

After the quantitative analyses, it was possible to confirm that the area occupied by the cells in CHT/K membranes had significantly increased when compared to cells seeded on CHT membranes, at every timepoint analysed.

3.2.2 Viability of relevant cell types in 2D cultures. The metabolic viability of several cell lines seeded in the CHT and CHT/keratin membranes was quantitatively determined by AB assay, as can be seen in Fig. 4 (left panels). For all cellular lines tested, there was an increase of fluorescence values in terms of relative fluorescence units (RFUs) with time, from day 1 to day 7, suggesting that the cells remained viable and an overall cellular proliferation occurred in both CHT and CHT/keratin samples. More specifically, the metabolic activity of BJ fibroblasts was significantly higher when seeded on keratin-based materials, both at day 3 and day 7, when compared to cells seeded in CHT membranes. The metabolic activity of

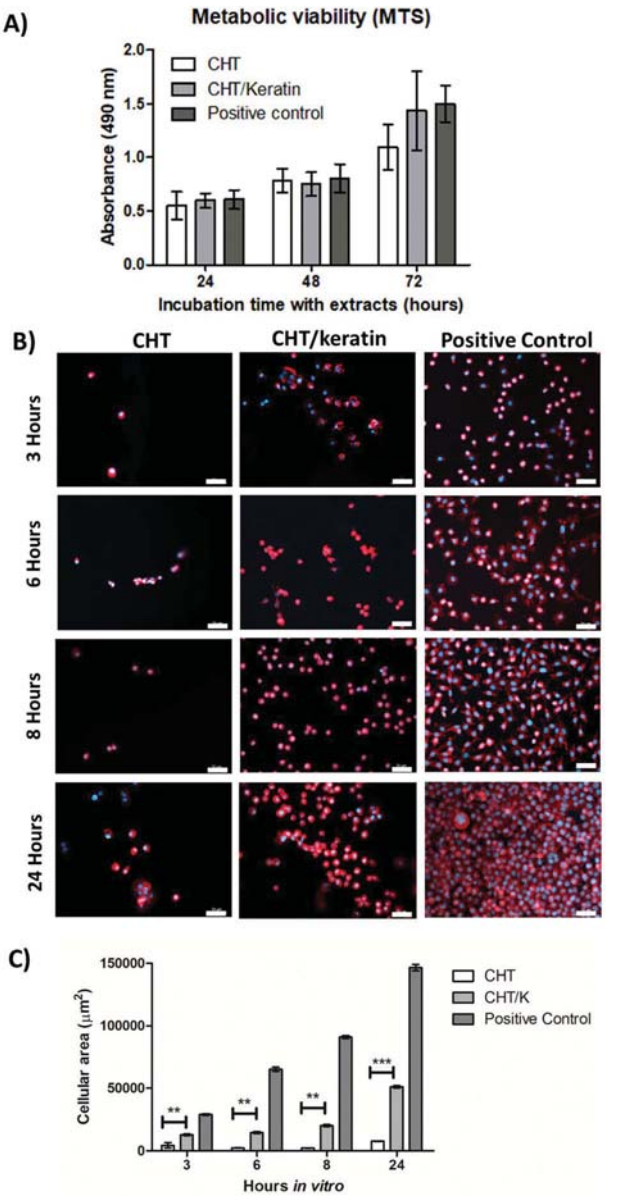

Fig. 3 Short term cytotoxicity screening and adhesion study with L929 fibroblasts. (A) Metabolic activity of L929 fibroblasts incubated with conditioned media (extracts) from CHT and CHT/keratin developed membranes. No statistically significant negative effect on the metabolic viability could be detected, in comparison with the positive control (monolayer of cells in TCPs with regular DMEM), after 14, 48 and 72 hours. Kruskal–Wallis test was performed followed by Dunn's multiple comparison test, $p < 0.05$. (B) Fluorescence photomicrographs for qualitative adhesion study where L929 fibroblasts were seeded on CHT and CHT/keratin membranes and compared to the positive control (TCPs). Cells were subjected to DAPI/phalloidin staining after fixation. Scale bar: 50 μm. (C) Quantitative adhesion study, where the cellular area occupied under each condition was measured. Mann Whitney test was performed, where $p < 0.05$.

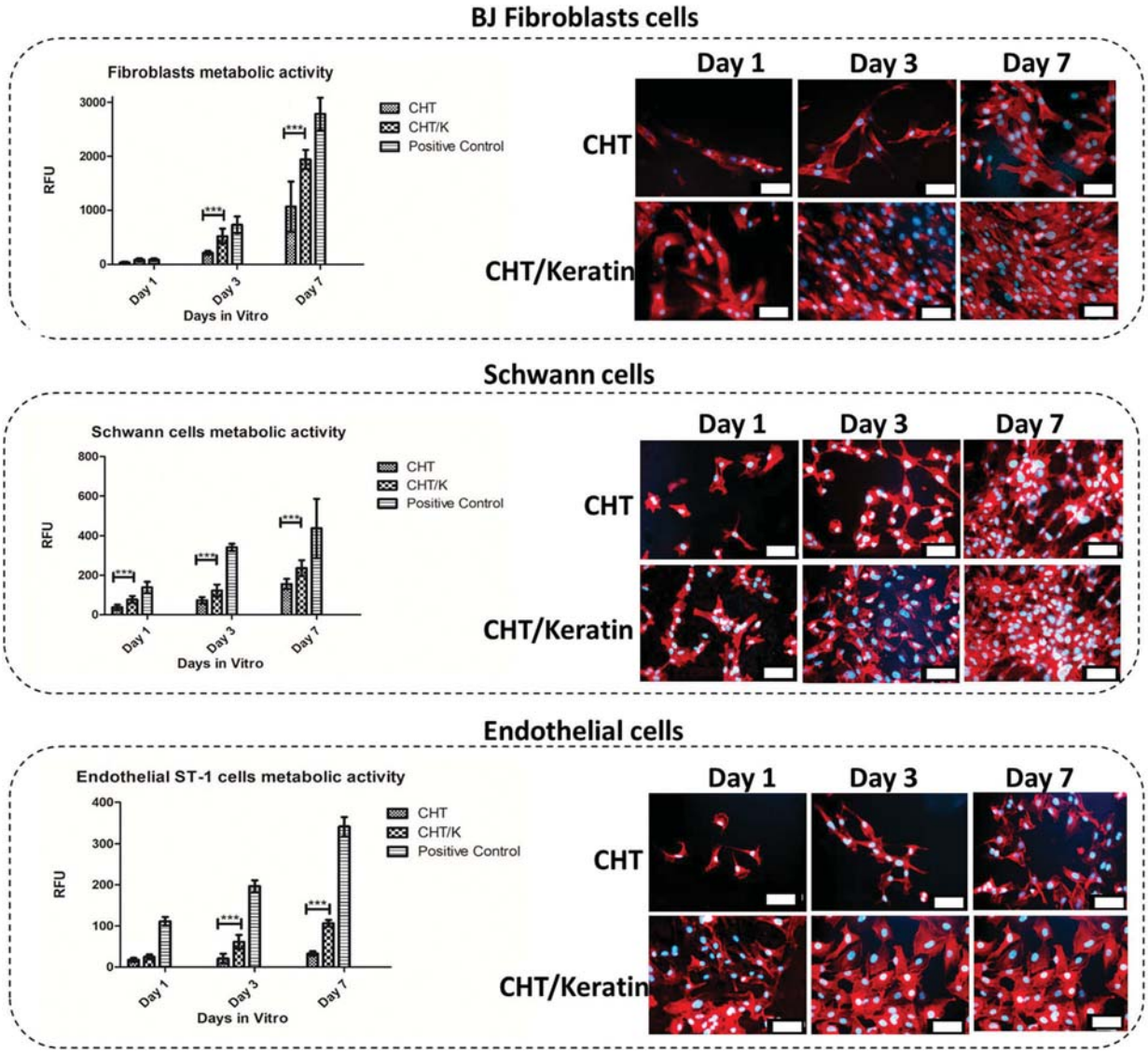

Fig. 4 Metabolic viability and cellular cytoskeleton morphology of BJ fibroblasts, Schwann cells and endothelial cells when seeded on CHT and CHT/keratin membranes, at 1, 3 and 7 days of culturing, comparing to the positive control (monolayer of cells in a TCP). Left: graphical representation of the quantification of metabolic activity of each cell type with up to 7 days of culturing. Right: fluorescence micrographs of DAPI/phalloidin stained cells, with up to 7 days of culturing. Scale bar: 50 μm.

Schwann cells was significantly higher in CHT/keratin membranes at all the timepoints analyzed (1, 3 and 7 days). Regarding endothelial cells, the determined metabolic activity was significantly higher in CHT/keratin materials after 3 and 7 days *in vitro*.

3.2.3 Cellular cytoskeleton morphology study of relevant cell lines. The cell morphologies of the different cell types were qualitatively analysed after DAPI/phalloidin staining at 1, 3 and 7 days of culturing (Fig. 4, right panels). The representative qualitative images are in accordance with metabolic activity determination, where an increased number of cells in CHT/keratin materials was observed when compared to that in CHT materials. Also, all cell types appeared to have their native morphologies.

3.3 *In vivo* angiogenic assay

Following the superior biological performance demonstrated by CHT/keratin membranes in *in vitro* studies, particularly on the significantly higher metabolic activity of the cultured endothelial cells, a CAM assay was performed to assess the effect of keratin addition on CHT membranes and make an association with their angiogenic response. After 4 days of implantation, the macroscopic assessment of the angiogenic response, based on the quantification of the convergent blood vessels toward the implanted materials, showed significant differences between the CHT/keratin and the simple CHT membranes. These findings can be seen in Fig. 5A, where it is clear that the statistically significant higher number of blood vessels con-

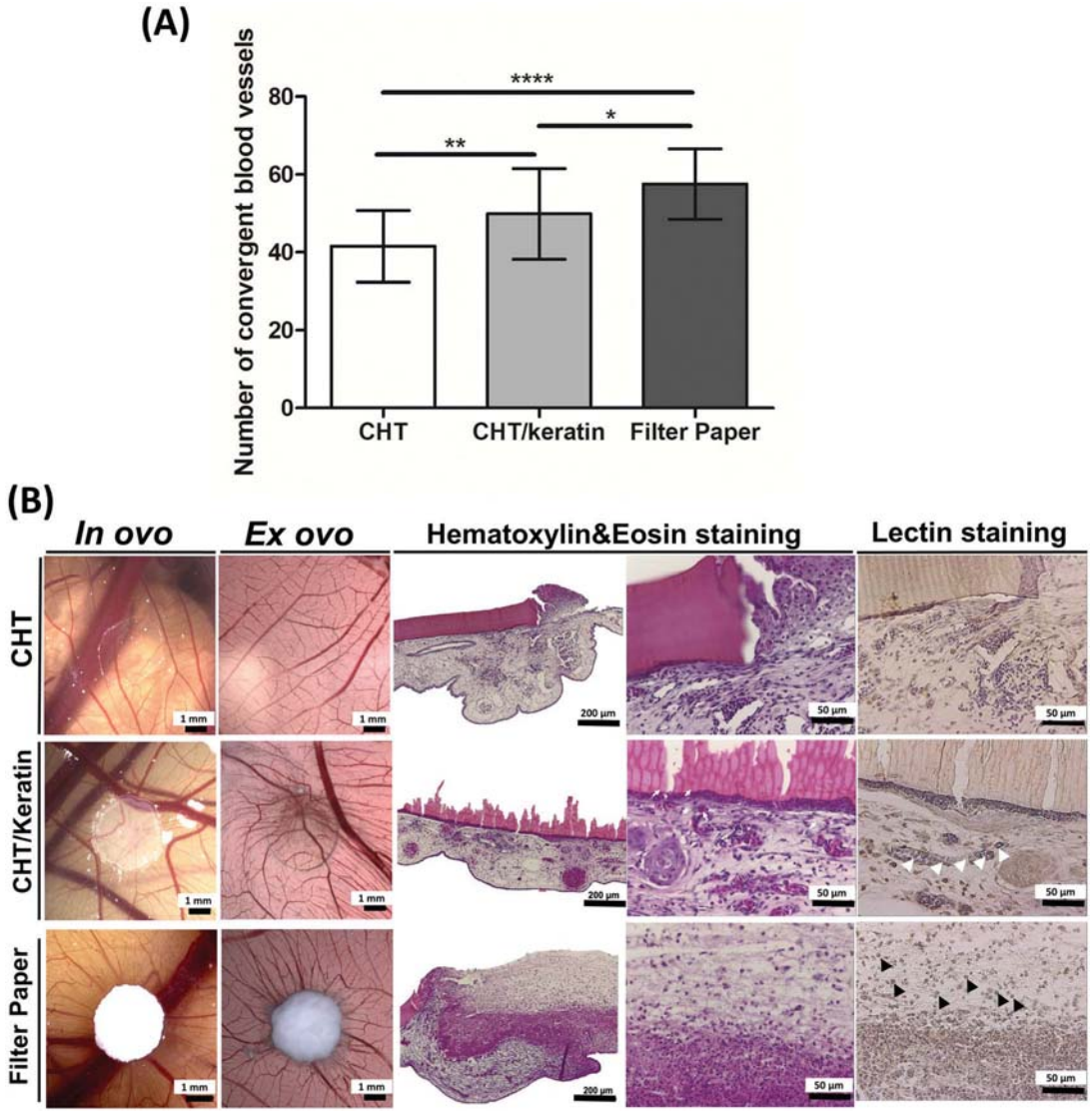

Fig. 5 Angiogenic response of the CHT-based membranes evaluated in the CAM assay. (A) Ex ovo quantification of the macroscopic blood vessels converging to the implanted CHT and CHT/keratin membranes and to the positive control filter paper, after 4 days of implantation. The mean number of convergent blood vessels with results from the counts of three independent observers of a minimum of 19 discs per implant. Statistical analysis was performed using one-way analysis of variance followed by Tukey's post-test. Symbols denote significant differences for $*p < 0.05$, $**p < 0.01$ and $****p < 0.0001$. (B) *In ovo* and *ex ovo* stereomicroscopy photographs of the CAM with the implanted materials after 4 days of implantation and light microcopy representative images of the respective 4 μm-sagittal CAM sections stained with H&E and lectin. The black arrows indicate infiltrated chick endothelial cells and the white arrows indicate the tendential migration of the erythrocytes and micro-vessels to the proximity of the CHT/keratin membranes.

verge to the CHT/keratin membranes compared to the CHT membranes ($**p < 0.01$ CHT/keratin *vs.* CHT). Both membranes exhibited a statistically significant lower number of convergent blood vessels when compared to the positive control, filter paper, the difference being less prominent for the CHT/keratin membranes. The microscopy study of the angiogenic response was performed by the histological characterization of representative CAM sections through H&E and lectin staining, the latter for the detection of chick origin-endothelial cells. The light microscopy images of the 4 μm-sagittal CAM sections depicted in Fig. 5B showed that both membranes were well integrated on the CAM. However, a slightly stronger adhesion of the CHT/keratin membranes to the CAM is noticeable. In such membranes, the presence of a morphologically related cellular interface was more often perceptible which can be attributed to a normal immune response to the implanted CHT/keratin membranes. However, no acute inflammatory response was observed, confirming the non-immunogenicity of the CHT-based membranes.

Nevertheless, the presence of a noticeable number of micro-vessels in the proximity of the CHT membranes could

be observed, being more pronounced on the CAM implanted with the keratin enriched membranes.

Moreover, this tendential preference of the newly formed micro-vessels towards the proximity of the CHT/keratin membranes could be observed from the migration of erythrocytes that seem to be arranging in new micro-vessels (marked by white arrows).

The integrity of both membranes was maintained during the implantation period. However, it is possible to microscopically observe that the CHT/keratin membranes present a more striated structure than CHT, which could retain its structure, after 4 days of implantation. These results are in agreement with the degradation studies. From observation from staining, it can be stated that the membranes were impermeable to cellular infiltration.

4 Discussion

GTR is a surgical technique developed for bone-related procedures, in which a physical barrier is used to regulate tissue growth.[51] However, this same principle is one of the most effective methods used for PNR. NGCs and PNWs are the most common strategies applied to stop fast-proliferating and collagen depositing fibroblasts from filling the injury site, while protecting it.[16,52]

An ideal NGC or PNW intended for PNR needs to feature a combination of optimal material, size, architecture and surface properties to be fully effective.[53] These features must allow the formation of a new ECM, consisting of endothelial cells, and subsequently blood vessels, Schwann cells and the correct type and amount of fibroblasts, which will collectively create favourable circumstances for nerve regeneration to occur.[54] In this study, we propose the use of solvent cast CHT/keratin membranes as possible tools to aid in the repair of damaged nerves.

Keratin has been recently extracted from human hair and has emerged as a captivating biomaterial.[55] This is because keratin is a human-derived protein, and exhibits excellent biocompatibility, no immune reaction upon transplantation, good cellular interaction activity and biodegradability.[56] In this case, the aim was to provide new desirable and improved characteristics to CHT membranes.[16] Making use of the previously developed 5% DA CHT membrane,[16] which were found to be optimal for PNR, we intended to study of the effect related to the addition of 1% of freeze-dried hair keratin.

CHT can be crosslinked by a variety of methods, such as the use of glutaraldehyde, formaldehyde, tripolyphosphate, genipin and/or vanillin.[57] However, in this experimental work, no crosslinking step was performed in the fabrication of the CHT membrane. Instead, the CHT powder was dissolved in an acidic solution (acetic acid, in which the NH_2 groups become protonated (NH_{3+})). After air drying for mold casting, the membranes were neutralized with sodium hydroxide, in order to neutralize the acidic solution. In this step of neutralization, the protonated amines become NH_2 again, stabilizing the membrane and making it water insoluble. There is no crosslinking, but a stabilization step at the moment of neutralization.

Regarding the keratin-containing materials, the production of the membranes was achieved by mixing the freeze-dried keratin powder with the previously prepared CHT solution (in acetic acid). On one hand, it has been described before that keratin powder has the ability to self-polymerize into an hydrogel when mixed with PBS.[25,26] On the other hand, extracted keratin proteins have an intrinsic ability to self-assemble and polymerize into porous, fibrous matrices.[55] This might be the phenomenon responsible for the highly rough and porous membrane obtained after the addition of keratin. Furthermore, literature research confirmed the possibility of self-assembling keratin in the presence of acetic acid, which confirms the likelihood of self-polymerization of keratin within the membranes, giving rise to such a topography.[58,59]

When blended, CHT and keratin were not crosslinked by any specific method, but simply mixed and solubilized in the acetic acid solution.

The surface topography evaluated by SEM and AFM revealed a significantly higher surface roughness in the presence of keratin, which might contribute to the advantageous characteristics of keratin containing membranes, since rougher materials have been linked to improved cellular behaviour.[60] Techniques such as FTIR, XRD and DSC were useful for confirming the success of the blending and proved that CHT and keratin are miscible polymers. The good miscibility between keratin and CHT may be attributed to intermolecular hydrogen bonding between CHT carbonyl groups and keratin amine groups.

The hydrophilicity of the ECM is one of the most noteworthy factors that directly affect cell adhesion in TE and is usually characterized by contact angle testing. The presence of keratin containing rich amino and carboxylic groups led to an improvement of the hydrophilicity and wettability of the CHT membrane, which has been reported before.[61] This is linked to the fact that keratin is a naturally hydrophilic protein.[56]

The capacity to react with water is also visible in the weight loss and water uptake properties of the CHT/keratin membranes. In agreement with other reports,[62] the presence of keratin in the polymer blend makes it more prone to react with water molecules, achieving higher swelling and degradation rates due to hydrolysis. However, despite a slightly higher degradation rate, only 6% of mass loss was observed after 30 days. As no enzyme (specifically lysozyme) was used in this assay, this can be attributed to the stability of the membranes. No specific crosslinking was performed in CHT; so there are no covalent links present in the structure. Therefore, hydrolysis is responsible for the determined weight loss. If any kind of crosslinking between free amino groups occurred, the newly created covalent bonds could exert a stabilizing effect on the polymer's structure, probably reducing its degradation. That is why we could determine degradation rates of 3 and 6% after 30 days, for CHT and CHT/K. Furthermore, the DA of CHT must also be considered. It is known that samples with a low degree of acetylation have a higher tendency to interact

with water molecules, due to free amine and hydroxyl groups.[7] There is a relationship between the swelling ability and degradation, as more interaction with water molecules leads to higher swelling and higher hydrolysis. With the incorporation of keratin, a hydrophilic molecule, the interaction with water increases, and therefore there is an increase in the degradation and swelling rates, as can be observed from the results. The mechanical properties of devices to be used in PNR, whether they are NGCs or PNWs, are of great importance for the repair to be successful. It is of special interest that the matrix is not only mechanically strong enough to withstand the pressure after implantation, but also deformable enough.[63] On one hand, the presence of keratin decreased the stiffness related to CHT membranes. On the other hand, its presence increased the capacity to disperse energy when subjected to a tensile force, by increasing the damping properties. To summarize, the incorporation of keratin changes the membrane's mechanical properties, which might be due to the presence of keratin protein interfering with the stability of the CHT solution, consequently decreasing its stiffness. This result is in accordance with previous reports.[64]

Since different cell types respond differently based on the substrate stiffness, it is known that cell behaviour can be improved if cultured in a mechanically favourable microenvironment.[65] As expected and previously reported in the literature, in a general way, nervous system cells prefer softer membranes,[65] which is the case of CHT/keratin membranes, presenting less stiffness. In this sense, it is expected that the presence of hair keratin will be beneficial in future PNR systems.

Knowing that different cell types play central roles in PNR, their interaction with the developed membrane was assessed in this experimental work, namely with fibroblasts, Schwann cells and endothelial cells.

The role of fibroblasts in the process of PNR has been controversial, with different opinions whether their presence is beneficial or harmful for nerve regeneration.[66] To achieve effective regeneration, an equilibrium must be reached so that nerve fibroblasts proliferate and contribute to tissue remodelling, but do not over-proliferate and create excessive scar tissue.

Schwann cells, which myelinate and ensheath nerve fibers in the peripheral nervous system, also secrete neurotrophins and produce ECM molecules, which facilitates nerve regeneration.[67] Furthermore, the basal lamina produced by Schwann cells after an injury is thought to be one of the main effector parts in PNR.

For the role of endothelial cells, increasing attention has been paid to the close relationship between tissue regeneration and angiogenesis, as the lack of blood supply is one of the important constraint factors hindering nerve regeneration.[68]

Overall, the biological *in vitro* results indicate that cellular behaviour was significantly improved when cells were seeded on CHT/keratin membranes, as opposed to that on CHT membranes.

In fact, the enhanced proliferation of cells is related to the fact that a higher adhesion occurred in the initial hours of cellular seeding in the CHT/K membranes. As more cells adhere and acquire their typical phenotype, they will be able to proliferate at a higher rate. The preliminary quantitative and qualitative tests on cellular adhesion allowed us to confirm the direct relationship between the important phenomena of early cellular adhesion and consequent proliferation, which significantly differs from CHT to CHT/K materials. The improvement in the attachment and proliferation of neuronal cells in the presence of keratin has already been demonstrated.[62] One explanation for such phenomena might be the existence of cell binding motifs in keratin extracted from hair, such as leucine-aspartic acid-valine (LDV) and glutamic acid-aspartic acid-serine (EDS) binding residues. These motifs are capable of supporting cellular attachment since they create a favourable matrix that permits cellular infiltration, attachment, proliferation and differentiation.[69] However, not only the cell binding motifs play a role in increased cellular attachment, but their increased surface roughness may be associated with maximal cell adhesion. Mechanical and hydrophilic properties, which were critically modified in the presence of keratin, will also have a direct effect on the ability of cellular adhesion, proliferation and differentiation.[70]

Since a statistically significant higher metabolic activity was found when endothelial cells were seeded in CHT/keratin membranes, it was relevant to perform a CAM assay investigating whether the presence of keratin in the materials would elicit a superior angiogenic response. The quantification of the macroscopic blood vessels converging toward the implanted membranes and the histological characterization of the explants suggest that the presence of keratin can have a chemotactic effect on the endothelial cells, promoting their tendential migration to the proximity of the CHT/keratin membranes. The positive effect of keratin on the angiogenic response of the CHT/keratin membranes was also reinforced by the statistically significant higher number of convergent blood vessels on the CAM implanted with CHT/keratin membranes, when compared to those with the free keratin CHT membranes. The hair-derived keratin effect on promoting angiogenesis has been reported in previous studies, for peripheral nerve regeneration and cardiac regeneration after myocardial infarction.[69] In fact, some epithelial keratins expressed under pathological conditions, such as cytokeratins 19 and 17, have been identified as stimulators of tumour angiogenesis development by interfering or activating some signalling pathways involved in cancer progression and metastasis.[71,72] These findings could unveil an underexplored potential of the hair-derived keratin for the development of new biomaterials for applications where angiogenesis is a crucial factor.

Given all the benefits found after the extensive characterization of CHT/keratin membranes, their use as GTR tools in PNR can be envisioned using different strategies, as can be seen in Fig. 6. This membrane has the following potential uses: (i) acting as a PNW around the damaged nerve,[73] protecting the site of nerve crush or repair by end-to-end surgery and avoiding post-operative nerve adhesion; (ii) bridging, as a NGC, the two nerve stumps after a severe peripheral nerve

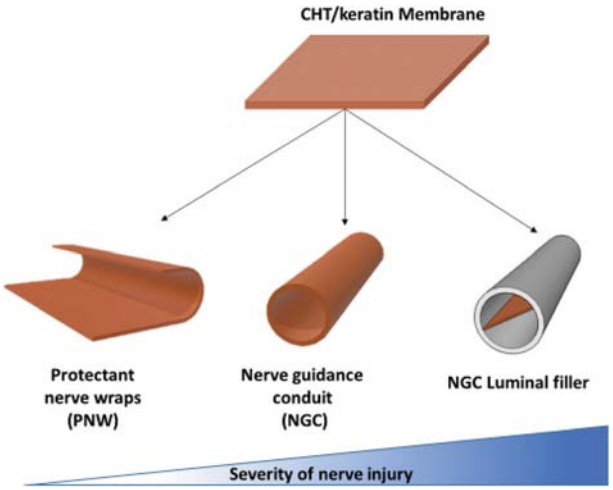

Fig. 6 The developed CHT/keratin membrane exhibited superior characteristics when compared to simple CHT membranes, both on a physico-chemical and on a biological level. When envisioned to be applied in peripheral nerve regeneration, different strategies can be used according to the severity of nerve injury. PNW should be used when the nerve is injured but the cable is intact. A NGC must be used when the nerve is severed and the result is a non-suturable gap. Finally, a luminal filler must be added to a NGC when the nerve cable cannot regenerate on its own due to the excessive long gap formed, and an extra guiding path is necessary for the nerve to reach the proximal side.

lesion with substance loss;[74] and (iii) acting as a luminal filler, where simple NGCs are enhanced by the introduction of a longitudinal membrane to reconstruct critical length injuries.[19] The choice of which strategy to use in clinics regarding the CHT/keratin membrane will mainly be dependent on the severity of the nerve injury. Regarding the first option, as the PNW, its use requires the nerve cable to be complete and the desirable qualities of a barrier nerve wrap include a biomaterial that decreases nerve scarring, does not constrict the nerve and improves nerve gliding. The NGC is necessary when the nerve is severed and there is a gap that needs to be protected from the remaining environment.[75] Finally, the CHT/keratin membrane could be used as a guiding luminal filler inside a NGC when the gap is critical, and the damaged nerve cannot regenerate without further support.[19]

5 Conclusions

In this work, the physicochemical and biological effects of incorporating human hair extracted keratin in 5% DA CHT membranes and its possible use as a GTR-based membrane were investigated. Surface and chemical characterization confirmed increased roughness and hydrophilicity with the addition of keratin, which pointed to an improved cellular behaviour. Furthermore, mechanical tests confirmed the suitability of the membrane to be applied in soft-tissue regeneration. *In vitro* biological assays established the membranes as non-cytotoxic, as well as being an appropriate matrix for several cellular types pertinent to nerve regeneration, such as fibroblasts, Schwann cells and endothelial cells. The CAM assay further proved the angiogenic potential of the developed CHT/keratin membrane blend and pointed to its advantageous effect in nerve repair. These results indicate the superior performance of CHT/keratin membranes, putting them in the perfect position to be further characterized *in vitro* and *in vivo*, with potential use in the scope of PNR.

Conflicts of interest

There are no conflicts to declare.

Acknowledgements

The authors are thankful for the chitosan raw material provided by Altakitin S.A. (Lisboa, Portugal). This study was also supported by the European Community's Seventh Framework Programme (FP7-HEALTH-2011) under grant agreement no. 278612 (BIOHYBRID). The authors acknowledge the Portuguese Foundation for Science and Technology (FCT) for the financial support provided to Joaquim M. Oliveira (IF/00423/2012 and IF/01285/2015) and Joana Silva-Correia (IF/00115/2015) under the program "Investigador FCT". The authors would also like to acknowledge the contribution of Elsa Ribeiro for the SEM image acquisition; Sandra Pina for the acquisition of XRD diffractograms; and Teresa Oliveira for histology sample processing.

References

1 M. C. Rodrigues, A. A. Rodrigues Jr., L. E. Glover, J. Voltarelli and C. V. Borlongan, *Sci. World J.*, 2012, **2012**, 413091.
2 J. Noble, C. A. Munro, V. S. Prasad and R. Midha, *J. Trauma Acute Care Surg.*, 1998, **45**, 116–122.
3 K. S. Taylor, D. J. Anastakis and K. D. Davis, *Pain*, 2010, **151**, 582–591.
4 R. Goswami, D. J. Anastakis, J. Katz and K. D. Davis, *Pain*, 2016, **157**, 729–739.
5 J. Scheib and A. Höke, *Nat. Rev. Neurol.*, 2013, **9**, 668.
6 R. Li, Z. Liu, Y. Pan, L. Chen, Z. Zhang and L. Lu, *Cell Biochem. Biophys.*, 2014, **68**, 449–454.
7 X. Jiang, S. H. Lim, H. Q. Mao and S. Y. Chew, *Exp. Neurol.*, 2010, **223**, 86–101.
8 M. C. Dodla, M. Alvarado-Velez, V. J. Mukhatyar and R. V. Bellamkonda, in *Principles of Regenerative Medicine*, ed. A. Atala, R. Lanza, A. G. Mikos and R. Nerem, Academic Press, Boston, 3rd edn, 2019, pp. 1223–1236, DOI: 10.1016/B978-0-12-809880-6.00069-2.
9 S. Yi, L. Xu and X. Gu, *Exp. Neurol.*, 2019, **319**, 112761.
10 K. Haastert-Talini, S. Geuna, L. B. Dahlin, C. Meyer, L. Stenberg, T. Freier, C. Heimann, C. Barwig, L. F. V. Pinto, S. Raimondo, G. Gambarotta, S. R. Samy,

N. Sousa, A. J. Salgado, A. Ratzka, S. Wrobel and C. Grothe, *Biomaterials*, 2013, **34**, 9886–9904.
11 R. Mali, P. Lele and Vishakha, *J. Indian Soc. Periodontol.*, 2011, **15**, 410–413.
12 K. Belanger, T. M. Dinis, S. Taourirt, G. Vidal, D. L. Kaplan and C. Egles, *Macromol. Biosci.*, 2016, **16**, 472–481.
13 A. R. Nectow, K. G. Marra and D. L. Kaplan, *Tissue Eng., Part B*, 2012, **18**, 40–50.
14 S. Gnavi, C. Barwig, T. Freier, K. Haastert-Talini, C. Grothe and S. Geuna, *Int. Rev. Neurobiol.*, 2013, **109**, 1–62.
15 A. Boecker, S. C. Daeschler, U. Kneser and L. Harhaus, *Front. Cell. Neurosci.*, 2019, **13**, 104.
16 C. R. Carvalho, R. Lopez-Cebral, J. Silva-Correia, J. M. Silva, J. F. Mano, T. H. Silva, T. Freier, R. L. Reis and J. M. Oliveira, *Mater. Sci. Eng., C*, 2017, **71**, 1122–1134.
17 K. Haastert-Talini, S. Geuna, L. B. Dahlin, C. Meyer, L. Stenberg, T. Freier, C. Heimann, C. Barwig, L. F. Pinto, S. Raimondo, G. Gambarotta, S. R. Samy, N. Sousa, A. J. Salgado, A. Ratzka, S. Wrobel and C. Grothe, *Biomaterials*, 2013, **34**, 9886–9904.
18 L. Stenberg, M. Stossel, G. Ronchi, S. Geuna, Y. Yin, S. Mommert, L. Martensson, J. Metzen, C. Grothe, L. B. Dahlin and K. Haastert-Talini, *BMC Neurosci.*, 2017, **18**, 53.
19 C. Meyer, L. Stenberg, F. Gonzalez-Perez, S. Wrobel, G. Ronchi, E. Udina, S. Suganuma, S. Geuna, X. Navarro, L. B. Dahlin, C. Grothe and K. Haastert-Talini, *Biomaterials*, 2016, **76**, 33–51.
20 S. Reichl, *Biomaterials*, 2009, **30**, 6854–6866.
21 S. Singaravelu, G. Ramanathan, M. D. Raja, N. Nagiah, P. Padmapriya, K. Kaveri and U. T. Sivagnanam, *Int. J. Biol. Macromol.*, 2016, **86**, 810–819.
22 J. K. Placone, J. Navarro, G. W. Laslo, M. J. Lerman, A. R. Gabard, G. J. Herendeen, E. E. Falco, S. Tomblyn, L. Burnett and J. P. Fisher, *Ann. Biomed. Eng.*, 2017, **45**, 237–248.
23 A. Tachibana, Y. Furuta, H. Takeshima, T. Tanabe and K. Yamauchi, *J. Biotechnol.*, 2002, **93**, 165–170.
24 H. Goto, K. Sawada and T. Fujisato, *Front. Bioeng. Biotechnol.*, DOI: 10.3389/conf.FBIOE.2016.01.02360.
25 P. Sierpinski, J. Garrett, J. Ma, P. Apel, D. Klorig, T. Smith, L. A. Koman, A. Atala and M. Van Dyke, *Biomaterials*, 2008, **29**, 118–128.
26 L. A. Pace, J. F. Plate, T. L. Smith and M. E. Van Dyke, *Biomaterials*, 2013, **34**, 5907–5914.
27 P. S. Hill, P. J. Apel, J. Barnwell, T. Smith, L. A. Koman, A. Atala and M. Van Dyke, *Tissue Eng., Part A*, 2011, **17**, 1499–1505.
28 L. A. Pace, J. F. Plate, S. Mannava, J. C. Barnwell, L. A. Koman, Z. Li, T. L. Smith and M. Van Dyke, *Tissue Eng., Part A*, 2014, **20**, 507–517.
29 P. Hartrianti, L. T. H. Nguyen, J. Johanes, S. M. Chou, P. Zhu, N. S. Tan, M. B. Y. Tang and K. W. Ng, *J. Tissue Eng. Regener. Med.*, 2017, **11**, 2590–2602.
30 F. Taraballi, S. Wang, J. Li, F. Y. Lee, S. S. Venkatraman, W. R. Birch, S. H. Teoh, F. Y. Boey and K. W. Ng, *Adv. Healthcare Mater.*, 2012, **1**, 513–519.
31 S. Wang, F. Taraballi, L. P. Tan and K. W. Ng, *Cell Tissue Res.*, 2012, **347**, 795–802.
32 R. França, D. A. Mbeh, T. D. Samani, C. Tien, M. A. Mateescu, L. H. Yahia and E. Sacher, *J. Biomed. Mater. Res., Part B*, 2013, **101**, 1444–1455.
33 R. Reichelt, *Science of Microscopy*, Springer, 2007, pp. 133–272.
34 M. Amrein, in *Science of Microscopy*, ed. P. W. Hawkes and J. C. H. Spence, Springer New York, New York, NY, 2007, pp. 1025–1069, DOI: 10.1007/978-0-387-49762-4_16.
35 T. Theophanides, *Infrared Spectroscopy-Materials Science, Engineering and Technology*, InTech, 2012.
36 P. Thibault, M. Dierolf, A. Menzel, O. Bunk, C. David and F. Pfeiffer, *Science*, 2008, **321**, 379–382.
37 V. I. Nizhenko, V. N. Eremenko and L. I. Sklyarenko, *Powder Metall. Met. Ceram.*, 1965, **4**, 463–466.
38 D. K. Owens and R. C. Wendt, *J. Appl. Polym. Sci.*, 1969, **13**, 1741–1747.
39 K. P. Menard and N. Menard, *Encyclopedia of Analytical Chemistry*, ed. R. A. Meyers, 2017, DOI: 10.1002/9780470027318.a2007.pub3.
40 C. Barreneche, A. Solé, L. Miró, I. Martorell, A. I. Fernández and L. F. Cabeza, *Thermochim. Acta*, 2013, **553**, 23–26.
41 M. B. Steed, V. Mukhatyar, C. Valmikinathan and R. V. Bellamkonda, *Atlas Oral Maxillofac. Surg. Clin. North Am.*, 2011, **19**, 119–130.
42 C. Oliveira, A. R. Costa-Pinto, R. L. Reis, A. Martins and N. M. Neves, *Biomacromolecules*, 2014, **15**, 2196–2205.
43 A. J. Salgado, O. P. Coutinho and R. L. Reis, *Tissue Eng.*, 2004, **10**, 465–474.
44 J. O'Brien, I. Wilson, T. Orton and F. Pognan, *Eur. J. Biochem.*, 2000, **267**, 5421–5426.
45 J. Silva-Correia, V. Miranda-Gonçalves, A. J. Salgado, N. Sousa, J. M. Oliveira, R. M. Reis and R. L. Reis, *Tissue Eng., Part A*, 2012, **18**, 1203–1212.
46 D. Ribatti, B. Nico, A. Vacca and M. Presta, *Nat. Protoc.*, 2006, **1**, 85–91.
47 H. Zheng, Y. Du, J. Yu, R. Huang and L. Zhang, *J. Appl. Polym. Sci.*, 2001, **80**, 2558–2565.
48 X.-F. Zheng, Q. Lian, H. Yang and X. Wang, *Sci. Rep.*, 2016, **6**, 21409.
49 P. P. Dhawade and R. N. Jagtap, *Adv. Appl. Sci. Res.*, 2012, **3**, 1372–1382.
50 H. M. Fahmy and M. M. Fouda, *Carbohydr. Polym.*, 2008, **73**, 606–611.
51 R. G. Caffesse, C. E. Nasjleti, A. E. Plotzke, G. B. Anderson and E. C. Morrison, *J. Periodontol.*, 1993, **64**, 1145–1153.
52 S. Wrobel, S. C. Serra, S. Ribeiro-Samy, N. Sousa, C. Heimann, C. Barwig, C. Grothe, A. J. Salgado and K. Haastert-Talini, *Tissue Eng., Part A*, 2014, **20**, 2339–2349.
53 C. R. Carvalho, J. B. Costa, A. da Silva Morais, R. López-Cebral, J. Silva-Correia, R. L. Reis and J. M. Oliveira, *Adv. Healthcare Mater.*, 2018, **7**, 1800186.
54 A. C. de Luca, S. P. Lacour, W. Raffoul and P. G. di Summa, *Neural Regener. Res.*, 2014, **9**, 1943–1948.

55 G. D. Mogosanu, A. M. Grumezescu and M. C. Chifiriuc, *Curr. Drug Targets*, 2014, **15**, 518–530.
56 T. R. Ham, R. T. Lee, S. Han, S. Haque, Y. Vodovotz, J. Gu, L. R. Burnett, S. Tomblyn and J. M. Saul, *Biomacromolecules*, 2016, **17**, 225–236.
57 V. A. Reyna-Urrutia, V. Mata-Haro, J. V. Cauich-Rodriguez, W. A. Herrera-Kao and J. M. Cervantes-Uc, *Eur. Polym. J.*, 2019, **117**, 424–433.
58 C. W. Lin, Y. K. Chen, M. Lu, K. L. Lou and J. Yu, *Polymers*, 2018, **10**, 987.
59 T. Tanabe, N. Okitsu, A. Tachibana and K. Yamauchi, *Biomaterials*, 2002, **23**, 817–825.
60 Z. Zhang, M. J. Gupte and P. X. Ma, *Expert Opin. Biol. Ther.*, 2013, **13**, 527–540.
61 H. Zhu, R. Li, X. Wu, K. Chen and J. Che, *Eur. Polym. J.*, 2017, **86**, 154–161.
62 P. Wu, X. Dai, K. Chen, R. Li and Y. Xing, *Int. J. Biol. Macromol.*, 2018, **114**, 1168–1173.
63 O. V. Cangellaris and M. U. Gillette, *Front. Mater.*, 2018, **5**, 21.
64 T. Tanabe, N. Okitsu, A. Tachibana and K. Yamauchi, *Biomaterials*, 2002, **23**, 817–825.
65 L. Ning, Y. Xu, X. Chen and D. J. Schreyer, *J. Biomater. Sci., Polym. Ed.*, 2016, **27**, 898–915.
66 L. Dreesmann, U. Mittnacht, M. Lietz and B. Schlosshauer, *Eur. J. Cell Biol.*, 2009, **88**, 285–300.
67 K. R. Jessen, R. Mirsky and A. C. Lloyd, *Cold Spring Harbor Perspect. Biol.*, 2015, **7**, a020487.
68 A. Abdal Dayem, M. K. Hossain, S. B. Lee, K. Kim, S. K. Saha, G.-M. Yang, H. Y. Choi and S.-G. Cho, *Int. J. Mol. Sci.*, 2017, **18**, 120.
69 D. Shen, X. Wang, L. Zhang, X. Zhao, J. Li, K. Cheng and J. Zhang, *Biomaterials*, 2011, **32**, 9290–9299.
70 A. R. Nectow, K. G. Marra and D. L. Kaplan, *Tissue Eng., Part B*, 2012, **18**, 40–50.
71 Y. Xu, S. Z. Zhang, C. H. Huang, X. Y. Liu, Z. H. Zhong, W. L. Hou, Z. F. Su and Y. Q. Wei, *BMB Rep.*, 2009, **42**, 344–349.
72 M. Takano, K. Shimada, T. Fujii, K. Morita, M. Takeda, Y. Nakajima, A. Nonomura, N. Konishi and C. Obayashi, *BMC Cancer*, 2016, **16**, 903.
73 A. E. Hasturk, E. R. Yilmaz, N. Hayirli, A. E. Kayalar, S. Akyildiz, E. C. Gökce, I. Akcay, O. Evirgen and A. Bakir, *J. Clin. Neurosci.*, 2018, **57**, 157–161.
74 S.-W. Peng, C.-W. Li, I.-M. Chiu and G.-J. Wang, *Int. J. Nanomed.*, 2017, **12**, 421–432.
75 M. Sarker, S. Naghieh, A. D. McInnes, D. J. Schreyer and X. Chen, *Biotechnol. J.*, 2018, **13**, e1700635.